Distributed Energy Management for Comprehensive Utilization of Residential Photovoltaic Outputs

Yu Fujimoto, Hiroshi Kikusato, *Student Member, IEEE*, Shinya Yoshizawa, *Member, IEEE*, Shunsuke Kawano, *Student Member, IEEE*, Akira Yoshida, Shinji Wakao, *Member, IEEE*, Noboru Murata, Yoshiharu Amano, Shin-ichi Tanabe, and Yasuhiro Hayashi, *Member, IEEE*

***Abstract*—The introduction of photovoltaic power systems is being significantly promoted. This paper proposes the implementation of a distributed energy management framework linking demand-side management systems and supply-side management system under the given time-of-use pricing program for efficient utilization of photovoltaic power outputs; each system implements a consistent management flow composed of forecasting, operation planning, and control steps. In our framework, demand-side systems distributed in the electric distribution network manage individual energy consumption to reduce the residential operating cost by utilizing the residential photovoltaic power system and controllable energy appliances so as not to inconvenience residents. On the other hand, the supply-side system utilizes photovoltaic power maximally while maintaining the quality of electric power. The effectiveness of the proposed framework is evaluated on the basis of an actual Japanese distribution network simulation model from both the supply-side and demand-side viewpoints.**

***Index Terms*—Energy management, photovoltaic power systems, forecasting, voltage control, cogeneration.**

NOMENCLATURE

Acronyms

EMS	Energy management system.
FC	Fuel cell cogeneration system.
FIT	Feed-in tariff.
GEMS	Grid energy management system.
HEMS	Home energy management system.
HV	High voltage (6,600[V]).
HVAC	Heating, ventilating and air conditioning system.
K-NN	K-nearest neighbor.
LDC	Line drop compensator.
LRT	Load-ratio control transformer.
LV	Low voltage (100-200[V])
LVR	Low-voltage regulator.
PV	Photovoltaic power system.
SVR	Step voltage regulator.
TOU	Time-of-use.

Symbols

α	Threshold for tap control in voltage regulator.
c	Cost conversion coefficients.
$\mathcal{D}$	Dataset.
$\overline{D}(\cdot), \underline{D}(\cdot)$	Cumulative difference measures between target voltage and voltage at regulating point.
$d(\boldsymbol{x}_1, \boldsymbol{x}_2)$	Distance between vectors $\boldsymbol{x}_1$ and $\boldsymbol{x}_2$.
$e(\cdot)$	Function for calculate electricity; e.g., $e_t^{\text{buy}}(\boldsymbol{\theta}_t \lfloor \boldsymbol{y})$ indicates purchased electricity under profile $\boldsymbol{y}$ at time t with parameter $\boldsymbol{\theta}_t$.
ε	Dead band parameter for vector-LDC control.
$g(\cdot)$	Function for calculation of gas consumption.
l	Line length.
$\mathcal{I}$	Set of forecast results in database.
$\dot{\boldsymbol{i}}_\tau(\boldsymbol{y})$	Complex vector of secondary current of target transformer at time τ under profile $\boldsymbol{y}$.
$J(\boldsymbol{\theta}\lfloor\boldsymbol{y})$	Daily cost function of operation parameter set $\boldsymbol{\theta}$ under given scenario $\boldsymbol{y}$ for demand-side EMS.
$\mathcal{J}$	Node index set in distribution network.
$\mathbb{E}_Y[\,\cdot\,]$	Expectation under various scenarios; e.g., $\mathbb{E}_Y[J(\boldsymbol{\theta}\lfloor Y)]$ indicates expected objective function of operation parameter set $\boldsymbol{\theta}$ for demand-side EMS.
K	Number of forecast results (scenarios).
$\boldsymbol{M}$	Positive-definite symmetric matrix (the Mahalanobis matrix).
M	Number of samples in database for demand forecast.
N	Number of samples in database for PV forecast.
$\mathcal{N}_K(\boldsymbol{x}_q; \mathcal{D})$	Index set of K-nearest neighbors of input query $\boldsymbol{x}_q$ in dataset $\mathcal{D}$.

Manuscript received November 4, 2015; revised March 4, 2016 and May 9, 2016; accepted June 8, 2016. Date of publication June 20, 2016; date of current version February 16, 2018. This work was supported by the Japan Science and Technology Agency Core Research for Evolutional Science and Technology Program. Paper no. TSG-01419-2015.

Y. Fujimoto is with the Advanced Collaborative Research Organization for Smart Society, Waseda University, Tokyo 169-8555, Japan (e-mail: y.fujimoto@aoni.waseda.jp).

H. Kikusato and S. Kawano are with the Graduate School of Advanced Science and Engineering, Waseda University, Tokyo 169-8555, Japan (e-mail: hiroshi-kikusato@akane.waseda.jp; shunsuke.kawano@ruri.waseda.jp).

S. Yoshizawa, S. Wakao, N. Murata, and Y. Hayashi are with the Department of Electrical Engineering and Bioscience, Waseda University, Tokyo 169-8555, Japan (e-mail: shin-yosi@fuji.waseda.jp; wakao@waseda.jp; mura@waseda.jp; hayashi@waseda.jp).

A. Yoshida is with the Graduate School of Fundamental Science and Engineering, Waseda University, Tokyo 169-8555, Japan (e-mail: yoshida@power.mech.waseda.ac.jp).

Y. Amano is with the Research Institute for Science and Engineering, Waseda University, Tokyo 169-8555, Japan (e-mail: yoshiha@waseda.jp).

S. Tanabe is with the Graduate School of Creative Science and Engineering, Waseda University, Tokyo 169-8555, Japan (e-mail: tanabe@waseda.jp).

Color versions of one or more of the figures in this paper are available online at http://ieeexplore.ieee.org.

Digital Object Identifier 10.1109/TSG.2016.2581882

$PMV(\theta)$	Predicted mean vote under parameter θ.
π	Prior probability.
$\mathcal{Q}$	Candidate set for vector-LDC parameter set.
$R(\boldsymbol{\psi}_t \vert \boldsymbol{y})$	Objective function of operation parameter set $\boldsymbol{\psi}_t$ under given scenario $\boldsymbol{y}$ for supply-side EMS.
$\tilde{R}(\boldsymbol{\psi} \vert \boldsymbol{y}^*)$	Objective value of parameter $\boldsymbol{\psi}$ under realization $\boldsymbol{y}^*$.
$r_K(\boldsymbol{x}_q; \mathcal{D})$	Distance between query $\boldsymbol{x}_q$ and its K-th nearest input in database $\mathcal{D}$.
s	Tap position of voltage regulator.
$S_\tau^p(\cdot)$	Amount of PV curtailment at point p in distribution network.
t	$\in \{1, \ldots, T\}$. Index of time slice.
τ	$\in \{1, \ldots, \mathrm{T}_t\}$. Index of dynamic control timing of GEMS in operation time slice t.
θ_0	Initial state of daily operation.
$\boldsymbol{\theta}$	$= \{\theta_1, \ldots, \theta_T\}$. Daily operation parameter set for operation of demand-side EMS which includes FC status (on/off), FC output, purchased electricity/gas, amount of reverse power flow from PV, and energy flow to advanced HVAC.
$\overline{v}, \underline{v}$	Upper and lower limits of appropriate voltage.
v	Scalar value of voltage.
$\dot{\boldsymbol{v}}_\tau(\boldsymbol{y})$	Complex vector of secondary voltage of target transformer at time τ under profile $\boldsymbol{y}$.
$\boldsymbol{x}$	Input vector used for forecast.
$\boldsymbol{y}$	$= (y_1, \ldots, y_T)$. Forecast target sequence.
$\boldsymbol{\psi}_t$	Parameter set of vector-LDC method at operation time slice t.
$\dot{\boldsymbol{z}}$	Complex vector of unit line impedance between transformer and regulating point.

Subscripts and Superscripts

$\cdot_t$	At the time slice t.
$\cdot_\tau$	At the arbitrary control timing τ.
$\cdot^e$	For calculating electricity.
$\cdot^g$	For calculating gas consumption.
$\cdot_i$	Of the i-th result in forecast result set $\mathcal{I}$.
$\cdot^j$	At node j.
$\cdot^{\mathrm{Ld}}$	For calculation of electricity demand.
$\cdot^{\mathrm{HW}}$	For calculation of hot water demand.
$\cdot^{\mathrm{PV}}$	For calculation of PV output.
$\cdot^{\mathrm{LDC}}$	For vector-LDC control.
$\cdot^{\mathrm{buy}}$	For calculation of purchased electricity.
$\cdot^{\mathrm{rev}}$	For calculation of reverse power flow.
$\cdot^{\mathrm{trg}}$	Of target.
$\cdot^{\mathrm{ref}}$	At the regulating point in distribution network.
$\cdot_k$	Of the k-th forecast result.
$\cdot_q$	Of query; e.g., $\boldsymbol{x}_q$ indicates query input.
$\cdot^*$	Realization; e.g., $\boldsymbol{y}^*$ indicates actual sequence.

I. Introduction

AFTER the Great East Japan Earthquake of 11 March, 2011, the introduction of residential PVs has been promoted significantly under the FIT program in Japan though the unexpected generation output fluctuation problem depending on the weather conditions becomes obvious. In this situation, demand-side energy management that achieves peak shift and saves non-essential energy consumption will play an important role [1], [2] in maintaining a stable balance between supply and demand; controllable residential energy appliances, e.g., FCs are expected to serve as a useful tool for providing an energy buffer to achieve efficient PV power utilization in demand-side energy management. One of the difficulties in demand-side energy management will be caused by the diversity in demand patterns due to the varying life styles of consumers. In situations where uncertainty in renewable energy sources begins to significantly affect the power system, the supply-side needs to maintain high power quality while taking into account the diversity in demand-side management results and utilizing renewable energy sources maximally. In order to handle the uncertainty in such a real-world system, various forecasting techniques for PV output [3], [4] and load [5], and robust energy appliance operation methods [6], [7] have been proposed in the energy informatics field. Particularly, in recent years, the idea of model predictive control [8] has been introduced for EMSs. Table I shows typical implementations of model predictive control for various EMSs [9]–[20]. As shown in the table, the framework has been applied both for demand-side and supply-side EMSs; the fact indicates that the framework of model predictive control is suitable for optimizing the global objective under the uncertainty of prediction results. However, in general, the supply-side and demand-side EMSs usually have their own objectives. Therefore, a framework for achieving globally suboptimal energy management under uncertainty according to the feasible real-world scheme by considering the difference in objectives for the demand-side and supply-side is required.

Here, the authors propose a framework of distributed EMSs that comprehensively utilizes outputs of distributed residential PV power systems to the fullest extent under the policy determined by given TOU pricing. The framework is consisting of a group of demand-side EMSs distributed in the electric distribution network and a supply-side EMS that affect each other; these two systems are briefly characterized as follows.

HEMS Demand-side EMS for consumers, managing controllable energy appliances to minimize residential operation cost (which is defined as the sum of electric power and gas supply charges in this paper) under the given TOU menu so as not to disturb residential thermal comfort.

GEMS Supply-side EMS in a distribution network for voltage support and reduction of PV curtailment by utilizing advanced voltage control devices.

The grid and home EMSs described in this paper are based on a consistent design principle based on three steps, i.e., *forecasting*, *operational plan*, and *control*, for handling uncertainty in PV outputs and variation in energy consumption patterns. The primary objectives of these systems are different, so that individual EMSs basically work for the implementer's benefit; however, residential PV outputs largely installed in a distribution network are expected to be utilized comprehensively by appropriately considering influence of the forecasting errors in the systems. In this paper, we introduce a method to derive

TABLE I
IMPLEMENTATIONS OF MODEL PREDICTIVE CONTROL FOR EMS

Reference	Purpose	Primary objective	Control Target
Camponogara et al. (2002) [9]	Supply-side EMS	Load frequency control in a power system	Generators
Houwing et al.(2009) [10]	Demand-side EMS	Operation cost under given electricity price	FC
Jin et al.(2010) [11]	Supply-side EMS	Voltage stabilization in a power system	Static var compensators
Arnold and Andersson (2011) [12]	Supply-side EMS	Operation costs of electricity and natural gas consumption in a power system	Multi-carrier energy systems consist of integrated electricity and natural gas systems
Oldewurtel et al. (2012) [13]	Demand-side EMS	Integrated room automation while respecting occupant comfort in a building	HVAC and blind positioning, etc.
Yamaguchi et al. (2013) [14]	Demand-side EMS	Residential operation costs of electricity	Battery of electric vehicles and plug-in hybrid vehicle
Kajgaard et al. (2013) [15]	Demand-side EMS	Residential operation costs of electricity	Electric heat pump load
Ziogou et al. (2013) [16]	Demand-side EMS	Safe and efficient demand tracking	FC
Monteiro and Igreja (2014) [17]	Supply-side EMS	Frequency regulation in a power system	Generators
Parisio et al. (2014) [18]	Supply/Demand-side EMS	Operation costs in a microgrid	Controllable loads, energy storage, and distributed generators
Su et al. (2014) [19]	Supply-side EMS	Operation costs in a distribution system	Power dispatches among distributed generators, energy storage systems, and advanced plug-in electric vehicles
Spudic et al. (2015) [20]	Supply-side EMS	Grid code compliance of wind farms	Wind farm controller

several plausible future demand and PV output curves in order to handle uncertainty in the forecast result, and propose a strategy to enjoy the advantage of this forecasting approach from the viewpoint of the expected value of the objective function in demand-side and supply-side EMSs. The proposed framework is implemented in our distributed EMS simulation model; we carry out numerical simulations of our EMS scheme based on a Japanese distribution network model, and evaluate the effectiveness of our proposed distributed framework from the viewpoints of the voltage violation, amount of curtailed PV outputs, and the demand-side operational cost simultaneously. Major contributions of this paper are briefly described as follows; (i) an idea of multiple scenario forecast is implemented for EMSs to treat uncertainty in forecast results, (ii) a demand-side EMS framework for minimization of operational cost is introduced, (iii) a supply-side EMS framework for reduction of voltage violation and PV curtailment is proposed, (iv) comprehensive impact of distributed EMS framework is evaluated from both perspectives of supply-side and demand-side simultaneously on the basis of an actual Japanese distribution network model, (v) effectiveness of advanced voltage control devices in supply-side EMS for reduction of voltage violation and PV curtailment is evaluated, and (vi) impact of forecasting errors in energy management is empirically evaluated.

The paper is composed as follows. In Section II, our proposed framework of distributed EMS is briefly described. Then, we introduce a framework of demand-side energy management system for home in Section III. Section IV also provides a supply-side energy management system for the distribution network. Simulation results of our proposed distributed EMS based on an actual Japanese distribution network are shown in Section V. Finally, Section VI is devoted to some concluding remarks.

II. FRAMEWORK OF DISTRIBUTED EMS

In this paper, we assume that the demand-side EMSs distributed in the power grid are introduced by energy consumers who may enjoy the benefits of sustainable residential operation cost reduction, and the supply-side EMS is introduced by a network operator; the operator takes responsibility for maintaining energy quality and enjoys the benefits of cost reduction by utilizing residential PV output instead of alternative power sources with expensive fuel cost. These independent systems are implemented to achieve their individual purposes while considering uncertainty in PV outputs and diversity in demand patterns so as to realize comprehensive utilization of the residential PV outputs by their ripple effects.

Fig. 1 shows a schematic image of our proposed distributed EMS framework which aims to reduce the expected voltage violation on the distribution network, the amount of curtailed PV output, and the expected operational cost for the consumers while keeping resident's thermal comfort through a TOU pricing program. Assume that the grid EMS provides a TOU pricing program to the consumers, and residential home EMS derives day-ahead operational plan of residential energy appliances in order to accomplish their local objectives, i.e., the minimization of the expected daily operation cost. Both grid and home EMSs are based on the following three steps; forecast, operational plan, and control. In the forecast step, the expected PV output and the expected energy consumption patterns are forecasted based on the database constructed in each system. Then, the appropriate operational parameter set for the forthcoming control period is derived based on the forecast result in the operational plan step. In the control step, the controllable appliances and devices are dynamically controlled according to the derived parameter set in order to mitigate the divergence between the current situation and the forecasting result.

Our proposed distributed energy management framework, shown in Fig. 1, works according to the following timeline. In the demand-side EMS, the quarter-hourly residential PV output and energy consumption for the forthcoming period from 3:00 to 27:00 are forecasted. Operation of several residential energy appliances is planned for the daily control according to the given TOU price until 3:00. In the supply-side EMS, the quarter-hourly total PV output and energy consumption of the target area for the next one hour are forecasted. Appropriate operational parameters for the hourly control of the voltage regulators are derived until the start of the control period.

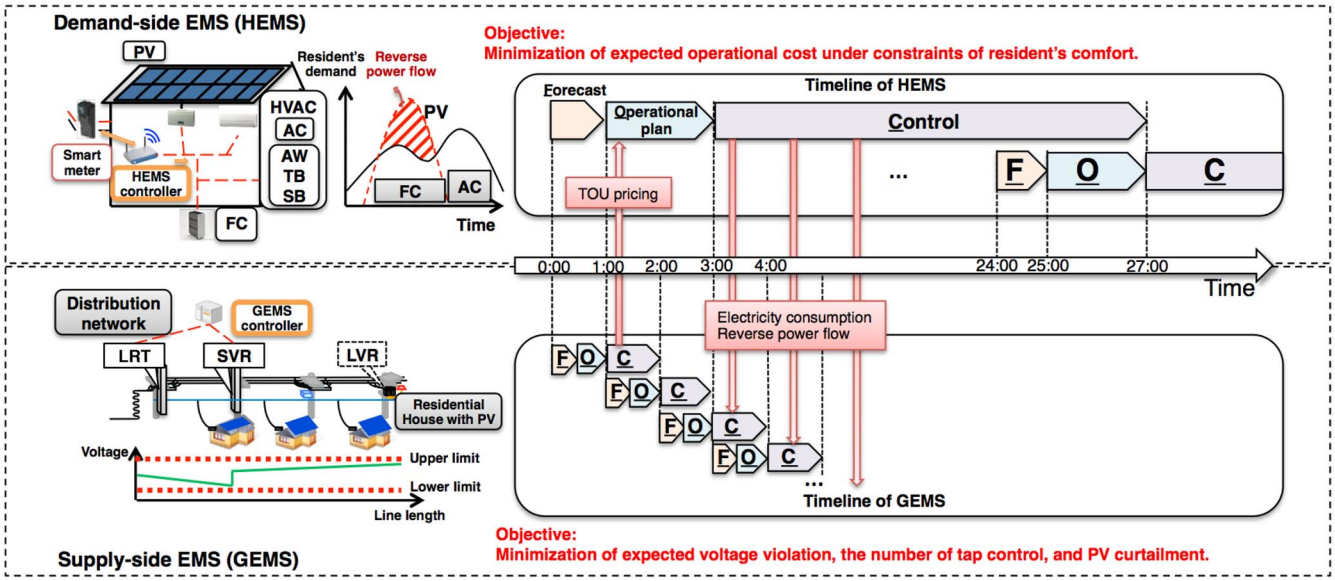

Fig. 1. Schematic image of distributed EMS framework. The GEMS aims to reduce the expected voltage violation in the distribution network, the number of tap controls, and the amount of curtailed PV output. The HEMS aims to reduce the expected operating cost for consumers while maintaining the resident's thermal comfort. Assume that the GEMS provides a TOU pricing program to the consumers, and the HEMS derives a day-ahead operational plan for residential energy appliances in order to reduce the expected daily operating cost. The control results of HEMSs affect the control of the GEMS through the change in energy consumption and reverse power flow from the residential PV.

Note that the control results of the demand-side EMSs distributed on the distribution network affect the control of the supply-side EMS through the change in energy consumption and reverse power flow from the residential PV.

III. Implementation of Demand-Side EMS

Now, we introduce an HEMS framework that is composed of an HEMS controller, a PV system, an FC system, and an advanced HVAC; we assume that the advanced HVAC includes the residential air-conditioning system, the automatic window, the thermal insulation automatic blind, and the sunlight shielding automatic blind. The proposed HEMS controller aims to plan a day-ahead schedule for energy appliances (FC status (on/off) and FC output for each time slice), the purchased electricity/gas, the amount of reverse power flow from the PV system, and energy flow to the advanced HVAC for minimizing the expected daily operating cost on the basis of the forecasted PV output and energy consumption under the constraint of thermal comfort. Fig. 2 shows the process flow of the demand-side EMS framework. The following subsections are devoted to the description of this procedure.

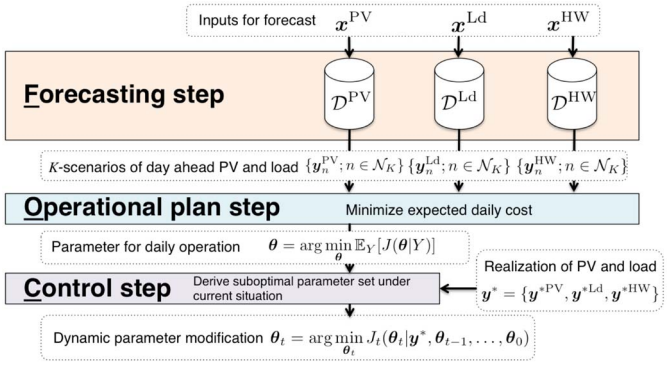

Fig. 2. Process flow of the demand-side EMS framework.

A. PV Forecast

At the forecasting step, we adopt the so-called just-in-time modeling scheme [21], [22], which achieves a nonparametric data-driven forecast and provides *multiple scenarios* as a set of plausible forecasting results [23] in order to achieve robust energy management in the presence of the forecasting errors caused by uncertainty in PV outputs and variation in residential loads. To implement the aforementioned idea, we focus on the following K-NN procedure. Let t be an index of the time slice in a day, $\boldsymbol{y}^{\mathrm{PV}} = (y_t^{\mathrm{PV}}; t \in \{1, \ldots, T\})$ be a sequence of PV outputs, and $\boldsymbol{x}_t^{\mathrm{PV}}$ be an input vector used to forecast the PV output at time t. We also let $\mathcal{D}_t^{\mathrm{PV}} = \{(\boldsymbol{x}_{n,t}^{\mathrm{PV}}, y_{n,t}^{\mathrm{PV}}); n \in \{1, \ldots, N\}, t \in \{1, \ldots, T\})\}$ be an input-output dataset used for forecasting the PV output at time t where N is the number of samples in the database $\mathcal{D}_t^{\mathrm{PV}}$. Here, T stands for the number of time slices to be forecasted; we focus on quarter-hourly daily profiles, so that $T = 96$ is used in our HEMS. We find the K-NNs of the input query $\boldsymbol{x}_q^{\mathrm{PV}}$ from the historical dataset $\{\boldsymbol{x}_{n,t}^{\mathrm{PV}}; n \in \{1, \ldots, N\}\}$ stored in $\mathcal{D}_t^{\mathrm{PV}}$, which is described as follows,

$$\mathcal{N}_K\left(\boldsymbol{x}_q^{\mathrm{PV}}; \mathcal{D}_t^{\mathrm{PV}}\right) = \left\{n \in \{1, \ldots, N\}; d\left(\boldsymbol{x}_q^{\mathrm{PV}}, \boldsymbol{x}_{n,t}^{\mathrm{PV}}\right) \leq r_K\left(\boldsymbol{x}_q^{\mathrm{PV}}; \mathcal{D}_t^{\mathrm{PV}}\right)\right\}, \quad (1)$$

where $d(\boldsymbol{x}_q^{\mathrm{PV}}, \boldsymbol{x}_{n,t}^{\mathrm{PV}})$ denotes the distance between the two input vectors $\boldsymbol{x}_q^{\mathrm{PV}}$ and $\boldsymbol{x}_{n,t}^{\mathrm{PV}}$, and $r_K(\boldsymbol{x}_q^{\mathrm{PV}}; \mathcal{D}_t^{\mathrm{PV}})$ indicates the distance between the query $\boldsymbol{x}_q^{\mathrm{PV}}$ and its K-th nearest input $\boldsymbol{x}^{\mathrm{PV}} \in \{\boldsymbol{x}_{n,t}^{\mathrm{PV}}; n \in \{1, \ldots, N\}\}$ in $\mathcal{D}_t^{\mathrm{PV}}$. For calculation of the

distance between input vectors to extract K-NNs given in (1), we use the following squared Euclidean distance:

$$d\left(\boldsymbol{x}_q^{\mathrm{PV}}, \boldsymbol{x}_{n,t}^{\mathrm{PV}}\right) = \left(\boldsymbol{x}_q^{\mathrm{PV}} - \boldsymbol{x}_{n,t}^{\mathrm{PV}}\right)\left(\boldsymbol{x}_q^{\mathrm{PV}} - \boldsymbol{x}_{n,t}^{\mathrm{PV}}\right)^{\top}. \tag{2}$$

By using the K-NNs, the multiple scenario forecast is achieved by returning the following set consisting of corresponding outputs,

$$\left\{y_{n,t}^{\mathrm{PV}}; n \in \mathcal{N}_K\left(\boldsymbol{x}_q^{\mathrm{PV}}; \mathcal{D}_t^{\mathrm{PV}}\right)\right\}. \tag{3}$$

Thus, the proposed framework outputs K plausible scenarios of PV output under the given condition $\boldsymbol{x}_q^{\mathrm{PV}}$. Note that the input vector $\boldsymbol{x}_{n,t}^{\mathrm{PV}}$ consists of the day length (sunrise-to-sunset), the sun's altitude at time t, and nine other weather prediction variables for t, provided as meso-scale model grid point values, the numerical weather prediction data provided by Japan meteorological business support center (http://www.jmbsc.or.jp/). The weather prediction variables used in our implementation are atmosphere pressure [hPa], wind velocity [m/s] (two directions), temperature [°C], humidity [%], cloudiness [%] (three elements), and rainfall [mm]. Note that all input variables are standardized by adopting linear transformation so that each variable takes a value between zero and one. These input variables are selected based on the Akaike's information criteria [24].

B. Demand Forecast

We also use the multiple scenario forecast framework for residential loads. Let $\boldsymbol{y}^{\mathrm{Ld}} = (y_t^{\mathrm{Ld}}; t \in \{1, \ldots, T\})$, $\boldsymbol{y}^{\mathrm{HW}} = (y_t^{\mathrm{HW}}; t \in \{1, \ldots, T\})$ be sequences of electricity demand and hot water demand; $\boldsymbol{x}^{\mathrm{Ld}}$, $\boldsymbol{x}^{\mathrm{HW}}$ be the corresponding input vectors; and $\mathcal{D}^{\mathrm{Ld}} = \{(\boldsymbol{x}_m^{\mathrm{Ld}}, \boldsymbol{y}_m^{\mathrm{Ld}}); m \in \{1, \ldots, M\}\}$, $\mathcal{D}^{\mathrm{HW}} = \{(\boldsymbol{x}_m^{\mathrm{HW}}, \boldsymbol{y}_m^{\mathrm{HW}}); m \in \{1, \ldots, M\}\}$ be input-output datasets used for forecasting electricity and hot water demand respectively where M is the number of samples in $\mathcal{D}^{\mathrm{Ld}}$ and $\mathcal{D}^{\mathrm{HW}}$. The plausible forecast results are derived in a similar fashion by selecting the K-NNs of the query $\boldsymbol{x}_q$; e.g., in the case of electricity load forecast,

$$\mathcal{N}_K\left(\boldsymbol{x}_q^{\mathrm{Ld}}; \mathcal{D}^{\mathrm{Ld}}\right) = \left\{m \in \{1, \ldots, M\}; d(\boldsymbol{x}_q^{\mathrm{Ld}}, \boldsymbol{x}_m^{\mathrm{Ld}}) \leq r_K\left(\boldsymbol{x}_q^{\mathrm{Ld}}; \mathcal{D}^{\mathrm{Ld}}\right)\right\}. \tag{4}$$

One of the difficulties in forecasting residential load is its diversity; the depth of the relationship between several explanatory variables and the demand differs from one household to another. In this paper, we take a scheme to learn the relative importance of each explanatory variable which is mainly acquired at the nearest weather station around the target house for forecasting the demand. To obtain plausible multiple forecast results for residential loads, we focus on the class of generalized squared Mahalanobis distance [25], which is given by

$$d\left(\boldsymbol{x}_q^{\mathrm{Ld}}, \boldsymbol{x}_m^{\mathrm{Ld}}\right) = \left(\boldsymbol{x}_q^{\mathrm{Ld}} - \boldsymbol{x}_m^{\mathrm{Ld}}\right)\boldsymbol{M}\left(\boldsymbol{x}_q^{\mathrm{Ld}} - \boldsymbol{x}_m^{\mathrm{Ld}}\right)^{\top}, \tag{5}$$

where $\boldsymbol{M}$ is a positive-definite symmetric matrix, the so-called Mahalanobis matrix. Note that the distance metric used in (5) is reduced to the Euclidean distance used in (2) if $\boldsymbol{M}$ is a unit matrix. Because it is important to reflect the effect of temporal variation in the daily energy consumption behavior quantitatively in the aforementioned distance metric, the appropriate matrix $\boldsymbol{M}$ is learned [23], [26] by using historical datasets $\mathcal{D}^{\mathrm{Ld}}$ and $\mathcal{D}^{\mathrm{HW}}$, respectively. Then, the multiple load scenario forecast is achieved by returning the outputs corresponding to (4) as follows,

$$\left\{\boldsymbol{y}_m^{\mathrm{Ld}}; m \in \mathcal{N}_K\left(\boldsymbol{x}_q^{\mathrm{Ld}}; \mathcal{D}^{\mathrm{Ld}}\right)\right\}. \tag{6}$$

On the basis of the aforementioned framework, we derive plausible K scenarios of the residential electricity load and those of the hot water demand under the given condition $\boldsymbol{x}_q^{\mathrm{Ld}}$ and $\boldsymbol{x}_q^{\mathrm{HW}}$. Note that the input vectors, $\boldsymbol{x}^{\mathrm{Ld}}$ and $\boldsymbol{x}^{\mathrm{HW}}$, are composed of quarter-hourly electricity (or hot water) demand [kWh/15 min] sequence of the previous day, and the hourly features of sea-level pressure [hPa], surface pressure [hPa], wind velocity [m/s] (two elements), temperature [°C], humidity [%], cloudiness [%] (four elements) and rainfall [mm] of the target day.

C. Demand-Side Energy Management Using Forecast

In our framework, the HEMS controller plans operations for dominant residential appliances so as to minimize the expected daily operating cost. We implement scenario-based stochastic optimization programming [27] by using the multiple-scenario forecast results of PV and load profiles [28] at the operational plan step; in this approach, we focus on optimizing the expected value of the objective function under several forecasted scenarios rather than the optimization under single scenario. We follow the setup of previous studies [28], [29] for appliance configuration and specific formulation policy for optimization, and focus on the essential optimization strategy in this paper. Let $\boldsymbol{\theta}_t$ be the set of parameters (decision variables) which includes the FC status (on/off), FC output, purchased electricity/gas, amount of reverse power flow from PV, and energy flow to the advanced HVAC at the time slice t. We also let $\boldsymbol{\theta} = \{\boldsymbol{\theta}_1, \ldots, \boldsymbol{\theta}_T\}$ be the daily operational plan which is composed of T feasible parameter subsets from the viewpoints of the energy and mass balances and the device states [28]. Assume that we can obtain the actual day-ahead PV outputs and demands $\boldsymbol{y}^* = \{\boldsymbol{y}^{*\mathrm{PV}}, \boldsymbol{y}^{*\mathrm{Ld}}, \boldsymbol{y}^{*\mathrm{HW}}\}$, the optimal operational plan for appliances is denoted as the following minimizer,

$$\begin{aligned}\boldsymbol{\theta}^* = \operatorname*{argmin}_{\boldsymbol{\theta}} \sum_{t=1}^{T} \Big(& c_t^e e_t^{\mathrm{buy}}(\boldsymbol{\theta}_t | \boldsymbol{y}^*, \boldsymbol{\theta}_{t-1}, \ldots, \boldsymbol{\theta}_0) \\ & + c_t^g g_t^{\mathrm{buy}}(\boldsymbol{\theta}_t | \boldsymbol{y}^*, \boldsymbol{\theta}_{t-1}, \ldots, \boldsymbol{\theta}_0) \\ & - c_t^{\mathrm{PV}} e_t^{\mathrm{rev}}(\boldsymbol{\theta}_t | \boldsymbol{y}^*, \boldsymbol{\theta}_{t-1}, \ldots, \boldsymbol{\theta}_0) \Big),\end{aligned} \tag{7}$$

where $\{c_t^e, c_t^g, c_t^{\mathrm{PV}}\}$ is the cost conversion coefficients, $\boldsymbol{\theta}_0$ indicates the initial state, and $e_t^{\mathrm{buy}}(\boldsymbol{\theta}_t | \boldsymbol{y}^*, \boldsymbol{\theta}_{t-1}, \ldots, \boldsymbol{\theta}_0)$, $g_t^{\mathrm{buy}}(\boldsymbol{\theta}_t | \boldsymbol{y}^*, \boldsymbol{\theta}_{t-1}, \ldots, \boldsymbol{\theta}_0)$, and $e_t^{\mathrm{rev}}(\boldsymbol{\theta}_t | \boldsymbol{y}^*, \boldsymbol{\theta}_{t-1}, \ldots, \boldsymbol{\theta}_0)$ are the purchased electricity, the gas consumption, and the reverse power flow from PV as functions of $\boldsymbol{\theta}_t$ under the previous parameter subset $\{\boldsymbol{\theta}_{t-1}, \ldots, \boldsymbol{\theta}_0\}$ and the realized profile $\boldsymbol{y}^*$. However, in general, we cannot access the actual day-ahead

profile set $\boldsymbol{y}^*$, so that we focus on the following daily operating cost function under the predicted scenario $\boldsymbol{y}_k$:

$$J(\boldsymbol{\theta}|\boldsymbol{y}_k) = \sum_{t=1}^{T}\Big(c_t^e e_t^{\text{buy}}(\boldsymbol{\theta}_t|\boldsymbol{y}_k, \boldsymbol{\theta}_{t-1}, \ldots, \boldsymbol{\theta}_0) + c_t^g g_t^{\text{buy}}(\boldsymbol{\theta}_t|\boldsymbol{y}_k, \boldsymbol{\theta}_{t-1}, \ldots, \boldsymbol{\theta}_0) - c_t^{\text{PV}} e_t^{\text{rev}}(\boldsymbol{\theta}_t|\boldsymbol{y}_k, \boldsymbol{\theta}_{t-1}, \ldots, \boldsymbol{\theta}_0)\Big). \quad (8)$$

The objective function used in our proposed daily operational planning method is given as the expectation of the daily operating cost (8), i.e.,

$$\begin{aligned} \min \quad & \mathbb{E}_Y[J(\boldsymbol{\theta}|Y)] \simeq \min \sum_{k=1}^{K} \pi_k J(\boldsymbol{\theta}|\boldsymbol{y}_k), \quad (9)\\ s.t. \quad & |PMV_t(\boldsymbol{\theta})| \le 0.5 \quad (\forall t), \end{aligned}$$

where $PMV_t(\boldsymbol{\theta})$ is the predicted mean vote [30], which is the index of the thermal comfort, at the time slice t, and π_k is the prior probability of the scenario $\boldsymbol{y}_k$; in our simulation, we set the uniform prior, i.e., $\pi_k = 1/K(\forall k)$. Specifically, $PMV_t(\boldsymbol{\theta})$ is predicted depending on the status of the advanced HVAC installed in the house (see the Appendix). Note that the introduction of the predicted mean vote index makes the optimization problem non-convex and nonlinear; in our problem setting, exogenous variable which expresses comfortable temperature range derived from $PMV_t(\boldsymbol{\theta})$ is introduced to avoid direct evaluation of the predicted mean vote. In our implementation, the scenarios are combined in accordance with the order of distance calculated in the K-NN selection at the forecast step; we make the k-th set $\boldsymbol{y}_k$ by combining the k-th nearest PV and demand scenarios from the query $\boldsymbol{x}_q$ for $k \in \{1, \ldots, K\}$.

In our framework, residential energy appliances are operated on the basis of the plan derived on the previous day. However, the results of the operation will be unsatisfactory when the PV outputs and demands differ from the forecasted results. Therefore, the FC output and the amounts of purchased electricity/gas are adjusted dynamically at the control step; the dynamic adjustment control is sequentially performed by using the following minimizer:

$$\begin{aligned} \boldsymbol{\theta}_t &= \underset{\boldsymbol{\theta}_t}{\text{argmin}}\, J_t(\boldsymbol{\theta}_t|\boldsymbol{y}^*, \boldsymbol{\theta}_{t-1}, \ldots, \boldsymbol{\theta}_0)\\ &= \underset{\boldsymbol{\theta}_t}{\text{argmin}}\Big\{c_t^e e_t^{\text{buy}}(\boldsymbol{\theta}_t|\boldsymbol{y}^*, \boldsymbol{\theta}_{t-1}, \ldots, \boldsymbol{\theta}_0) + c_t^g g_t^{\text{buy}}(\boldsymbol{\theta}_t|\boldsymbol{y}^*, \boldsymbol{\theta}_{t-1}, \ldots, \boldsymbol{\theta}_0) - c_t^{\text{PV}} e_t^{\text{rev}}(\boldsymbol{\theta}_t|\boldsymbol{y}^*, \boldsymbol{\theta}_{t-1}, \ldots, \boldsymbol{\theta}_0)\Big\}, \quad (10) \end{aligned}$$

which is derived by employing mixed-integer linear programming. Note that the set of sequential minimizers shown in (10) do not correspond to the solution of the global optimization problem shown in (7) because of situation-dependent constraints caused by the residential appliances.

IV. Implementation of Supply-Side EMS

Our supply-side management framework is composed of a GEMS controller and voltage regulators such as an LRT and an SVR (see Fig. 1). Furthermore, we employ the LVR which is a pole transformer with an auto tap changer for controlling the voltage in the low-voltage distribution system as an option for an advanced GEMS.

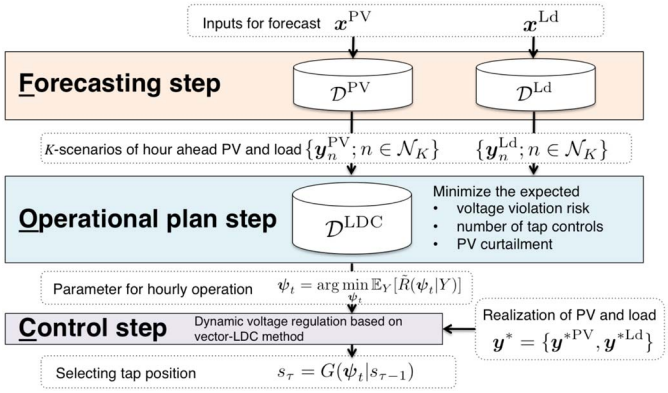

Fig. 3. Process flow of the supply-side EMS framework.

Fig. 3 shows the process flow of the supply-side EMS framework. At the forecasting step, the quarter-hourly sequence of aggregated PV outputs and electricity demands of the voltage control target area are forecasted every hour on the basis of the just-in-time modeling according to (3) and (6). Note that we focus on hourly profiles in our GEMS.

A. Supply-Side Energy Management Using Forecast

At the control step, the tap ratios of the LRT, SVR, and LVR are controlled using the framework called the vector-LDC method [31]. In this method, a regulator monitors its secondary voltage and current to control the tap dynamically. Let $\dot{\boldsymbol{v}}_\tau(\boldsymbol{y}^*)$ and $\dot{\boldsymbol{i}}_\tau(\boldsymbol{y}^*)$ be the secondary voltage and current of the target transformer at the arbitrary timing τ under the actual total PV outputs and demands $\boldsymbol{y}^* = \{\boldsymbol{y}^{*\text{PV}}, \boldsymbol{y}^{*\text{Ld}}\}$. The voltage regulator controls the tap position to keep the voltage at the regulating point v_τ^{ref} by monitoring $\dot{\boldsymbol{v}}_\tau(\boldsymbol{y}^*)$ and $\dot{\boldsymbol{i}}_\tau(\boldsymbol{y}^*)$. In the vector-LDC scheme, the voltage at the regulating point v_τ^{ref} at the arbitrary timing τ is estimated according to the following equation:

$$v_\tau^{\text{ref}}(l) = \left|\dot{\boldsymbol{v}}_\tau(\boldsymbol{y}^*) - l\dot{\boldsymbol{z}}\dot{\boldsymbol{i}}_\tau(\boldsymbol{y}^*)\right|. \quad (11)$$

Note that $\dot{\boldsymbol{z}}$ in (11) indicates the unit line impedance and l is the line length between the transformer and the regulating point. Let $\overline{D}_\tau(\boldsymbol{\psi}_t)$ and $\underline{D}_\tau(\boldsymbol{\psi}_t)$ be the cumulative differences between target voltage v_t^{trg} and v_τ^{ref} with the dead band ε, i.e.,

$$\overline{D}_\tau(\boldsymbol{\psi}_t) = \max\Big\{0, \overline{D}_{\tau-1}(\psi_t) + v_\tau^{\text{ref}}(l) - v_t^{\text{trg}} - \varepsilon\Big\}, \quad (12)$$

$$\underline{D}_\tau(\boldsymbol{\psi}_t) = \max\Big\{0, \underline{D}_{\tau-1}(\psi_t) + v_t^{\text{trg}} - \varepsilon - v_\tau^{\text{ref}}(l)\Big\}, \quad (13)$$

where $\boldsymbol{\psi}_t = \{v_t^{\text{trg}}, l\}$ is a parameter set of the vector-LDC method at the operation time slice t. In our framework, the tap position s_τ at the control timing τ under the parameter $\boldsymbol{\psi}_t$ is controlled according to the values defined in (12) and (13) as follows,

$$s_\tau = G(\psi_t|s_{\tau-1}) = \begin{cases} s_{\tau-1} + 1, & \text{if } \underline{D}_\tau(\boldsymbol{\psi}_t) > \alpha,\\ s_{\tau-1} - 1, & \text{if } \overline{D}_\tau(\boldsymbol{\psi}_t) > \alpha,\\ s_{\tau-1}, & \text{otherwise,} \end{cases} \quad (14)$$

where α indicates the given threshold; in our implementation, we use a typical real-world value, $\alpha = 30[\% \cdot \mathrm{s}]$, for all voltage regulators. If the tap position is regulated, the cumulative voltage differences $\overline{D}_\tau(\psi_t)$ and $\underline{D}_\tau(\psi_t)$ are reset to zero.

Now, we focus on the determination of the operational parameter set $\boldsymbol{\psi}_t$ for the time slice t. Assume that the operation time slice t is composed of $\tau \in \{1, \ldots, \mathrm{T}_t\}$ dynamic control timings. Let $v_\tau^j(\boldsymbol{\psi}_t|\boldsymbol{y}^*)$ be the voltage at the node $j \in \mathcal{J}$ under the given parameter $\boldsymbol{\psi}_t$ and $\boldsymbol{y}^*$ where $\mathcal{J}$ is the index set of nodes in the distribution network. We also let $\overline{v}^j$ and $\underline{v}^j$ be the upper and lower limits of the appropriate voltage at the node j. The optimal LDC parameter is ideally expressed under the realized $\boldsymbol{y}^*$ as follows:

$$\begin{aligned}\boldsymbol{\psi}_t^* &= \operatorname*{argmin}_{\boldsymbol{\psi}_t} R\big(\boldsymbol{\psi}_t|\boldsymbol{y}^*\big) \\ &= \operatorname*{argmin}_{\boldsymbol{\psi}_t} \Bigg\{ \sum_{j\in\mathcal{J}} \sum_{\tau=1}^{\mathrm{T}_t} h\big(v_\tau^j\big(\boldsymbol{\psi}_t|\boldsymbol{y}^*\big); \overline{v}^j, \underline{v}^j\big) \\ &\qquad + c_1 \sum_{\tau=1}^{\mathrm{T}_t} |s_{\tau+1} - s_\tau| + c_2 \sum_{p\in\mathcal{P}} \sum_{\tau=1}^{\mathrm{T}_t} S_\tau^p\big(\boldsymbol{\psi}_t|\boldsymbol{y}^*\big) \Bigg\},\end{aligned} \tag{15}$$

where

$$h\big(v_\tau^j; \overline{v}^j, \underline{v}^j\big) = \begin{cases} v_\tau^j - \overline{v}^j, & \text{if } v_\tau^j > \overline{v}^j \\ \underline{v}^j - v_\tau^j, & \text{if } v_\tau^j < \underline{v}^j \\ 0, & \text{if } \underline{v}^j \le v_\tau^j \le \overline{v}^j, \end{cases}$$

and $S_\tau^p(\boldsymbol{\psi}_t|\boldsymbol{y}^*)$ is the amount of PV curtailment at the point $p \in \mathcal{P}$ in the distribution network. The first term in (15) indicates the cumulative amount of voltage violations, the second term indicates the cumulative number of tap controls derived in (14), and the third term indicates the cumulative amount of PV curtailment, respectively. The function $R(\boldsymbol{\psi}_t|\boldsymbol{y}^*)$ evaluates the result of the operation under parameters $\boldsymbol{\psi}_t$ and $\boldsymbol{y}^*$, so that it is calculated on the basis of the power flow simulation. However we cannot again access the actual $\boldsymbol{y}^*$, and therefore we focus on the following expected minimization problem by using the multiple prediction scenarios $\{\boldsymbol{y}_k\}$,

$$\min \mathbb{E}_Y[R(\boldsymbol{\psi}_t|Y)] \simeq \min \sum_{k=1}^{K} \pi_k R(\boldsymbol{\psi}_t|\boldsymbol{y}_k), \tag{16}$$

where $\pi_k = 1/K(\forall k)$ is the uniform prior. The function $R(\boldsymbol{\psi}_t|\boldsymbol{y}_k)$ in the minimization problem (16) is calculated by power flow simulation with voltage regulator models, which in general requires high computational cost.

B. Data-Driven Parameter Selection for Scalable Implementation

To solve the computational cost problem, we derive the appropriate parameter $\boldsymbol{\psi}_t$ depending on the majority voting results of the plausible parameter candidates based on the nearest neighbor of the forecasted profiles $\{\boldsymbol{y}_k\}$ stored in the database [32]. Let $\mathcal{I} = \{1, \ldots, I\}$ be the set of forecast results in the database and $\mathcal{Q} = \{1, \ldots, Q\}$ be the set of candidates for the parameter set. Let

$$\mathcal{D}^{\mathrm{LDC}} = \big\{\big(\tilde{\boldsymbol{y}}_i, \boldsymbol{\psi}_q, \tilde{R}_i\big(\boldsymbol{\psi}_q|\boldsymbol{y}_i^*\big)\big); i \in \mathcal{I}, q \in \mathcal{Q}\big\}, \tag{17}$$

be the database of the size $I \times Q$ used for the determination of the LDC parameter, which is composed of a triplet consisting of the historical forecast result $\tilde{\boldsymbol{y}}_i$ whose realization is $\boldsymbol{y}_i^*$, an LDC parameter set $\boldsymbol{\psi}_q$, and the objective value $\tilde{R}_i(\boldsymbol{\psi}_q|\boldsymbol{y}_i^*)$ which indicates the evaluation result of the parameter $\boldsymbol{\psi}_q$ under the realization $\boldsymbol{y}_i^*$, i.e.,

$$\begin{aligned}\tilde{R}_i\big(\boldsymbol{\psi}_q|\boldsymbol{y}_i^*\big) = \Bigg\{ &\sum_{j\in\mathcal{J}} \sum_{\tau=1}^{\mathrm{T}_t} h\big(v_\tau^j\big(\boldsymbol{\psi}_q|\boldsymbol{y}_i^*\big); \overline{v}^j, \underline{v}^j\big) \\ &+ c_1 \sum_{\tau=1}^{\mathrm{T}_t} |s_{\tau+1} - s_\tau| + c_2 \sum_{p\in\mathcal{P}} \sum_{\tau=1}^{\mathrm{T}_t} S_\tau^p\big(\boldsymbol{\psi}_q|\boldsymbol{y}_i^*\big) \Bigg\}.\end{aligned} \tag{18}$$

Note that $\tilde{R}_i(\boldsymbol{\psi}_q|\boldsymbol{y}_i^*)$ stored in the database (17) can be calculated from the off-line power flow simulation, so that the computational cost does not become an issue. In our proposed framework, the nearest profile $\tilde{\boldsymbol{y}}_{\mathcal{N}_1(\boldsymbol{y}_k;\mathcal{D}^{\mathrm{LDC}})}$ for a forecast result $\boldsymbol{y}_k$ is selected from the database $\mathcal{D}^{\mathrm{LDC}}$. Finally, the parameter $\boldsymbol{\psi}_t$ is determined by minimizing the expectation of the objective function (18) on the basis of the forecasted scenarios, i.e.,

$$\begin{aligned}\boldsymbol{\psi}_t &= \operatorname*{argmin}_{\boldsymbol{\psi}_q} \mathbb{E}_Y\big[\tilde{R}(\boldsymbol{\psi}_q|Y)\big] \\ &\simeq \operatorname*{argmin}_{\boldsymbol{\psi}_q} \sum_{k=1}^{K} \pi_k \tilde{R}_{\mathcal{N}_1(\boldsymbol{y}_k;\mathcal{D}^{\mathrm{LDC}})}\Big(\boldsymbol{\psi}_q|\boldsymbol{y}^*_{\mathcal{N}_1(\boldsymbol{y}_k;\mathcal{D}^{\mathrm{LDC}})}\Big).\end{aligned} \tag{19}$$

Note that (19) reflects the effect of forecast errors in historical data and yields the appropriate operational parameter without using online power flow calculation for a large number of LDC parameter candidates under multiple scenarios.

We adopt our proposed parameter determination scheme for LRT and SVR at the operational plan step.

V. Numerical Experiments

To evaluate the effectiveness of our proposed distributed framework linking HEMSs and GEMS from the standpoints of the residential operating cost, total amount of curtailed PV output, and cumulative amount of voltage violation, we perform some numerical case studies on the basis of 30 days (January 2008) of real-world PV output and energy demand profiles with a time step of 10 [s] by using a distribution network model [33] which simulates an actual Japanese 6.6 [kV] distribution power system (Fig. 4). The model installs an LRT on the distribution substation, and an SVR on the feeder. We assume that all the 479 residential customers distributed in the low-voltage area install residential PV systems. We also assume that HEMSs are installed in 42 houses at the terminal area of the feeder. In this numerical experiments, thermal comfort $PMV_t(\boldsymbol{\theta})$ in each house is calculated based on thermal simulation by using the residential space model [28], a

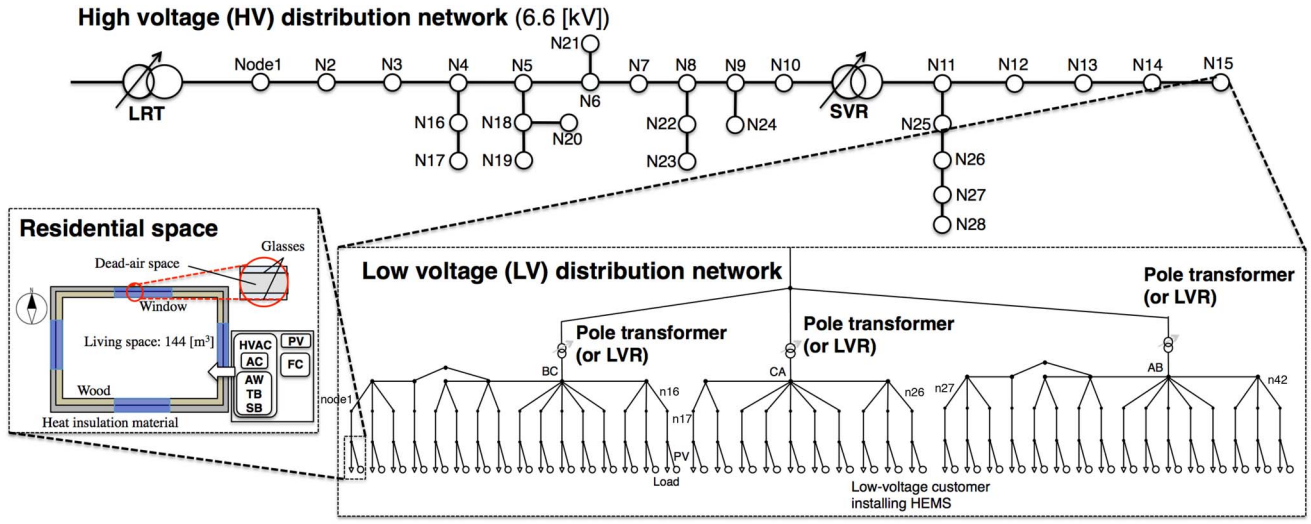

Fig. 4. Schematic image of the simulation model. The model installs an LRT on the distribution substation, and an SVR on the feeder. Assume that all the 479 residential customers distributed in the low-voltage area install residential PV systems. We also assume that HEMSs are installed in 42 houses at the terminal area of the feeder; thermal comfort $PMV_t(\boldsymbol{\theta})$ in each house is calculated based on thermal simulation by using the residential space model [28], a typical air-conditioning system model [34], and actual ambient temperature data acquired during the period of focused 30 days.

TABLE II
SIMULATION SETUP

Distribution network model	Line length	10.5 [km]
	Load capacity	2,971 [kVA]
	Acceptable HV range	6,557 - 6,879 [V]
	Acceptable LV range	95 - 107 [V]
Parameters of LRT	Tap width	60 [V]
	Dead band	1.0 [%]
	candidates for v_t^{trg}	$\{6480, 6510, ..., 6870\}$ [V]
	candidates for l	$\{0.0, 0.5, ..., 10.5\}$ [km]
Parameters of SVR	Tap width	100 [V]
	Dead band	1.5 [%]
	candidates for v_t^{trg}	$\{6480, 6510, ..., 6870\}$ [V]
	candidates for l	$\{0.0, 0.5, ..., 4.5\}$ [km]
Parameters of LVR	Tap width	2.38 [V]
	Dead band	1.5 [%]
	v_t^{trg}	101 [V]
	l	0 [km]
Spec of PV inverters	Curtailment starting voltage	107 [V]
	Curtailment ending voltage	106.5 [V]
	Speed of curtailment	0.02 [kW/s]
Spec of FC	Rated power output	0.75 [kW]
	Rated heat recovery	1.08 [kW]
	Efficiency of electric heater	95 [%]
	Tank volume	0.147 [m^3]
	Thermal loss of tank	1.7 [%/h]
	Efficiency of back-up boiler	92 [%]
Data acquisition period for DB	$\mathcal{D}^{\mathrm{Ld}}$	Jan. 1st - Dec. 31st in 2007
	$\mathcal{D}^{\mathrm{PV}}$	Jan. 1st - Dec. 31st in 2007

TABLE III
ELECTRICITY AND GAS RATE

Electricity rate	TOU pricing	07:00-13:00	28.99 [yen/kWh]
		13:00-16:00	54.68 [yen/kWh]
		16:00-23:00	28.99 [yen/kWh]
		23:00-07:00	12.16 [yen/kWh]
	Basic rate		1296 [yen/month]
	Feed-in-Tariff		37.00 [yen/kWh]
Gas rate	Basic rate		1458 [yen/month]
	Unit rate		134.51 [yen/Nm^3]

typical air-conditioning system model [34], and actual ambient temperature data acquired during the period of focused 30 days. Table II shows our experimental setup including several dominant parameters, and Table III shows electricity and gas rate used for derivation of residential operation cost; we assumed a current real-world TOU menu provided by Tokyo Electric Power Company Holdings, Inc. In this experiment, demand-side optimization problems are solved by CPLEX optimizer [35] with the default setting and the off-line power flow simulation is calculated on the basis of the add-on tool for MATLAB [36] which was developed under the JST CREST program [33].

In this simulation, we assess the effect of the distributed EMS framework in a step-by-step manner; we especially focus on evaluating the effectiveness of

- the proposed HEMS (pHEMS) by a comparison with the conventional management (cHEMS), which adopts the predetermined operation schedule without using forecast results and performs the dynamic adjustment control,
- the proposed GEMS (pGEMS) by a comparison of the conventional management (cGEMS), whose operation follows the predetermined fixed operation parameters,
- low-voltage regulators at the terminal node where the 42 HEMSs are installed for the advanced supply-side management (pGEMS with LVR),

under the assumption that all 42 houses installing the HEMS have an FC. In the cHEMS, we assume that the FC generates electricity from 04:00 to 24:00. In this simulation, we also evaluate the effectiveness of our EMS framework based on multiple scenario forecast under $K = 5$ by comparing with the latest EMS framework which implements the idea of model predictive control (with $K = 1$).

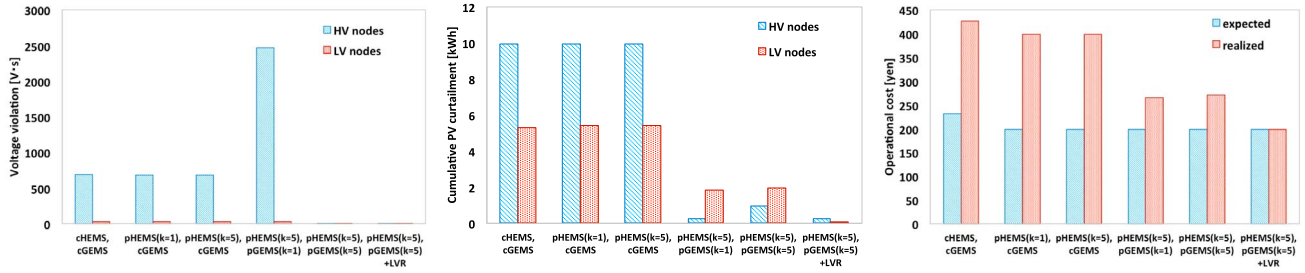

(a) Cumulative voltage violation (b) PV curtailment (c) Operational cost

Fig. 5. Simulation results: daily averages of (a) the cumulative voltage violation, (b) the PV curtailment per household, and (c) operating cost per household.

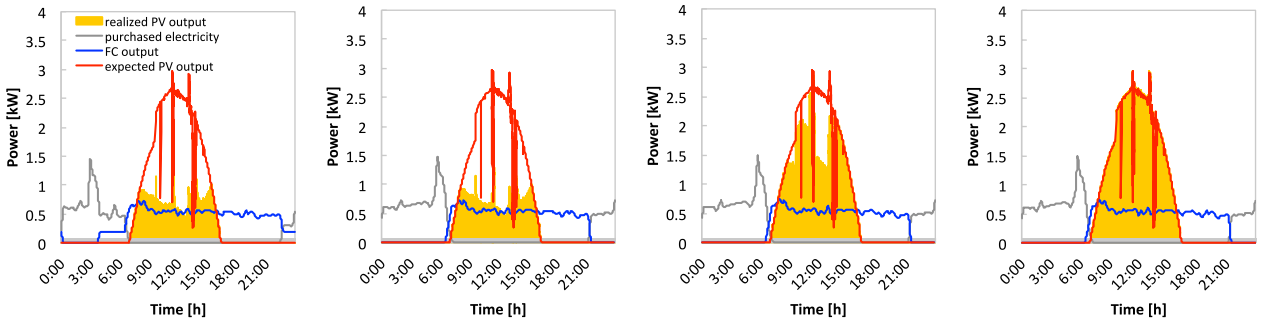

(a) cHEMS under cGEMS (b) pHEMS under cGEMS (c) pHEMS under pGEMS (d) pHEMS under pGEMS with LVR

Fig. 6. An example of demand-side management; profiles of (a) the scheduled FC operation without using forecasting under the cGEMS, (b) the pHEMS ($K = 5$) under the cGEMS, (c) the pHEMS under the pGEMS ($K = 5$), and (d) the pHEMS under the pGEMS with LVR. The cumulative difference between the expected and realized PV outputs corresponds to the amount of daily PV curtailment occurring in this house.

Fig. 5 shows the simulation results; daily averages of the cumulative voltage violation at the high voltage nodes and the low voltage nodes (Fig. 5(a)), daily averages of the PV curtailment per household connected to the high voltage nodes (N1-N14) and the focused low voltage nodes (n1-n42) (Fig. 5(b)), and daily averages of the expected and the realized operating cost per household (Fig. 5(c)). The results show that the HEMS framework based on model predictive control (pHEMS with $K = 1$) achieves to reduce the realized operational cost 28.298 [yen/day] from the conventional HEMS. The realized operational cost is slightly improved by our proposed HEMS based on the multiple scenario forecast scheme with $K = 5$; the numerical results imply that our proposed HEMS effectively avoids to the expected cost by considering the uncertainty of the forecast result. Compared with the expected operational cost under the assumption that the surplus PV output is sold as planned in HEMS, the realized operational cost deviates significantly. The results also indicate that the average PV curtailment is drastically reduced at the high voltage nodes (9.96[kWh] $\rightarrow$ 0.29[kWh]) and the operating cost is improved by introducing predictive control framework into the GEMS (pGEMS with $K = 1$); this is attributed to the increase of the opportunity that PV selling is enabled. By contrast, cumulative voltage violation at the high voltage nodes is remarkably worsen (683.2[V $\cdot$ s] $\rightarrow$ 2464.1[V $\cdot$ s]); this is attributed to lower limit deviation. Our proposed supply-side framework based on multiple scenario forecast (pGEMS with $K = 5$) achieves to reduce the expected risk of voltage violation (2464.1[V $\cdot$ s] $\rightarrow$ 0.3[V $\cdot$ s]) by considering uncertainty in the forecast results. The introduction of the LVRs at the low voltage distribution network (see Fig. 4) tolerate the active cost-driven operation plans given in demand-side and support quality maintenance of the power supply from the viewpoint of voltage; the results show that PV curtailment, particularly occurred at low voltage nodes, is substantially reduced (1.97[kWh] $\rightarrow$ 0.01[kWh]) and imply that the effectiveness of distributed energy management by utilizing residential PV output comprehensively.

An example of the demand-side management results, i.e., the FC profile, realized/expected PV output, and purchased electricity is shown in Fig. 6; Fig. 6(a) shows the profiles of the cHEMS (scheduled FC operation without using forecasting) under the cGEMS, Fig. 6(b) shows those of the pHEMS with $K = 5$, Fig. 6(c) shows the profiles of the pHEMS under the pGEMS with $K = 5$, and Fig. 6(d) shows those of the pHEMS under the pGEMS with LVR. Note that the cumulative difference between the expected and realized PV outputs corresponds to the amount of daily PV curtailment occurring in this house. Fig. 6(b) implies that the FC is operated according to the forecast results so as to reduce the operating cost, while the PV output is curtailed significantly because the voltage in this area remains in a critical state under the cGEMS. As shown in the figure, the amount of curtailed PV output is significantly reduced under the proposed GEMS. The results also suggest that the introduction of the LVR further mitigates the problem of PV curtailment.

Fig. 7 shows an example of node voltage profiles of the conventional GEMS and the proposed GEMS with the LVR

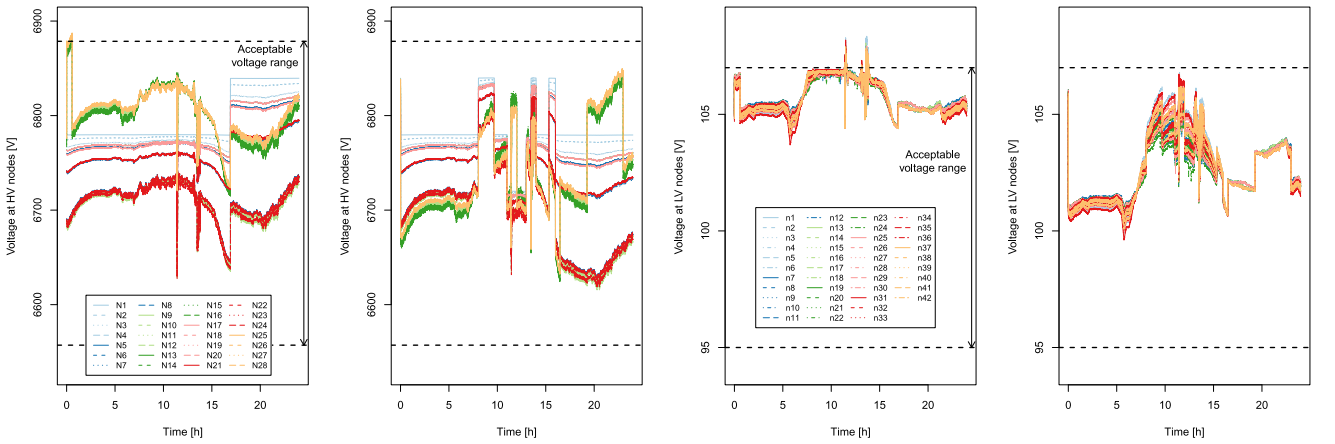

(a) HV profiles under cGEMS (b) HV profiles under pGEMS w. LVR (c) LV profiles under cGEMS (d) LV profiles under pGEMS w. LVR

Fig. 7. Voltage profiles of the cGEMS and the pGEMS ($k = 5$) with LVR under the pHEMS; profiles at (a) HV nodes under the cGEMS, (b) HV nodes under the pGEMS with LVR, (c) LV nodes under the cGEMS and (d) LV nodes under the pGEMS with LVR.

under the proposed HEMS. Figs. 7(a) and (c) indicate that voltage values sometimes exceed the upper limit of the acceptable range at both high and low voltage nodes under the cGEMS even when some PV output is curtailed. On the other hand, Figs. 7(b) and (d) show that node voltage values are controlled within the acceptable range under the pGEMS by using LVR. The results show that the proposed GEMS framework controls voltage within the acceptable range.

We should note that the computational time for optimization at the operational plan step in the demand-side EMS is almost linear with respect to the number of forecast scenarios K. In the numerical experiments, the computational time is $1,233[s]$ (about 21[min]) under $K = 5$ by using single-thread processing. A method for LDC parameter derivation introduced in Section IV-B also realizes fast implementation of the operational plan step in the supply-side EMS; in the experiments, the LDC parameter set is derived in several seconds. These results show a scalability of the proposed method for the real-world implementation.

The simulation results imply that the proposed distributed EMS framework achieves a synergistic effect for utilization of the PV output by minimizing the expected operating cost under the given TOU menu from the demand-side perspective and by reducing the expected voltage violation risk from the supply-side perspective.

VI. Conclusion

In this paper, we propose a distributed energy management framework between demand-side EMSs and a supply-side EMS for comprehensive utilization of distributed residential PV systems; each EMS is composed of a consistent management flow based on forecast, operational plan, and control steps. In particular, this paper proposes the EMS framework based on multiple scenario forecast and scenario-based stochastic optimization programming to mitigate the effects of prediction errors which cannot be corrected in the naive implementation of the latest EMS framework based on model predictive control. We also evaluate the effectiveness of a distributed EMSs under the given TOU pricing by using a distribution network simulation model from the viewpoints of operational cost, voltage violation, and total PV curtailment. The simulation results imply that the proposed EMS framework based on the idea of multiple scenario forecast achieves a synergistic effect for utilization of the PV output by minimizing expected operational cost under the given TOU menu from the demand-side perspective and by reducing expected voltage violation risk from the supply-side perspective.

We have implemented the proposed framework under the assumption that the timing of parameter updating is predetermined individually for each system; further investigation will be needed to determine the appropriate updating cycle in distributed EMSs. This paper focused only on the use of FCs and HVACs in the demand-side EMS; however, various residential energy appliances should be used for comprehensive utilization of residential PV outputs; verification of the effectiveness of the distributed EMS framework by using various residential home appliances will be an important topic, though it remains as a future work. In the supply-side EMS, we particularly focused on voltage issue as a constraint on a comprehensive utilization of the PV output, however, operation results of demand-side EMS also affect the energy losses in power systems. Application of our framework by cooperating with the other kind of GEMS scheme from the viewpoint of loss reduction will provide an important information for grid operators. Investigation of the effects of our proposed scheme from the loss perspective, and development of a method to cooperate with GEMS for the purpose of loss reduction are the topics of our research in progress.

Appendix

Let M be the metabolic rate [W/m^2], W be the effective mechanical power [W/m^2], I_{cl} be the clothing insulation [m$^2\cdot$ K/W], f_{cl} be the clothing surface area factor, $t_a(\theta)$ be the air temperature [°C] under the operation parameter θ, $\bar{t}_r$ be the mean radiant temperature, v_{ar} be the relative air velocity [m/s], p_a is the water vapor partial pressure [Pa], h_c be the

convective heat transfer coefficient [W/(m^2·K)], and t_{cl} be the clothing surface temperature [°C]. The predicted mean vote index $PMV_t(\theta)$ used in HEMS optimization (9) is explicitly given as follows:

$$\begin{aligned} &PMV_t(\theta) \\ &\quad = (0.303\exp(-0.036\cdot M)+0.028) \\ &\qquad \cdot\Big[(M-W)-3.05\cdot 10^{-3}(5733-6.99(M-W)-p_a) \\ &\qquad -0.42((M-W)-58.15)-1.7\cdot 10^{-5}M(5867-p_a) \\ &\qquad -0.0014M(34-t_a(\theta))-f_{cl}h_c(t_{cl}-t_a(\theta))) \\ &\qquad -3.96\cdot 10^{-8}f_{cl}\Big((t_{cl}+273)^4-\big(\bar{t}_r+273\big)^4\Big)\Big], \end{aligned}$$

where

$$\begin{aligned} t_{cl} &= 35.7-0.028(M-W)-I_{cl}\Big(3.96\cdot 10^{-8}f_{cl} \\ &\quad \cdot\Big((t_{cl}+273)^4-\big(\bar{t}_r+273\big)^4\Big)+f_{cl}h_c(t_{cl}-t_a(\theta))\Big), \end{aligned}$$

$$h_c = \begin{cases} 2.38|t_{cl}-t_a(\theta)|^{0.25}, \\ \qquad \text{if } 2.38|t_{cl}-t_a(\theta)|^{0.25} \geq 12.1\sqrt{v_{ar}} \\ 12.1\sqrt{v_{ar}}, \\ \qquad \text{if } 2.38|t_{cl}-t_a(\theta)|^{0.25} < 12.1\sqrt{v_{ar}}, \end{cases}$$

$$f_{cl} = \begin{cases} 1.00+1.290I_{cl}, & \text{if } I_{cl} \leq 0.078\big[m^2\cdot K/W\big] \\ 1.05+0.645*I_{cl}, & \text{if } I_{cl} > 0.078\big[m^2\cdot K/W\big]. \end{cases}$$

REFERENCES

[1] Y. Ozturk, D. Senthilkumar, S. Kumar, and G. Lee, "An intelligent home energy management system to improve demand response," *IEEE Trans. Smart Grid*, vol. 4, no. 2, pp. 694–701, Jun. 2013.

[2] G. Brusco, A. Burgio, D. Menniti, A. Pinnarelli, and N. Sorrentino, "Energy management system for an energy district with demand response availability," *IEEE Trans. Smart Grid*, vol. 5, no. 5, pp. 2385–2393, Sep. 2014.

[3] C. W. Chow *et al.*, "Intra-hour forecasting with a total sky imager at the UC San Diego solar energy testbed," *Solar Energy*, vol. 85, no. 11, pp. 2881–2893, 2011.

[4] H. T. C. Pedro and C. F. M. Coimbra, "Assessment of forecasting techniques for solar power production with no exogenous inputs," *Solar Energy*, vol. 86, no. 7, pp. 2017–2028, 2012.

[5] R. Weron, *Modeling and Forecasting Electricity Loads and Prices: A Statistical Approach* (Wiley Finance Series). Hoboken, NJ, USA: Wiley, 2006.

[6] Y. Zhou, C. Wang, B. Jiao, and Y. Wang, "Robust load scheduling in a smart home with photovoltaic system," *Energy Proc.*, vol. 61, pp. 772–776, May 2015.

[7] E. Kuznetsova, C. Ruiz, Y.-F. Li, and E. Zio, "Analysis of robust optimization for decentralized microgrid energy management under uncertainty," *Elect. Power Energy Syst.*, vol. 64, pp. 815–832, Jan. 2015.

[8] A. Bemporad and M. Morari, "Robust model predictive control: A survey," in *Robustness in Identification and Control* (Lecture Notes in Control and Information Sciences), vol. 245. London, U.K.: Springer, 1999, pp. 207–226.

[9] E. Camponogara, D. Jia, B. H. Krogh, and S. Talukdar, "Distributed model predictive control," *IEEE Control Syst.*, vol. 22, no. 1, pp. 44–52, Feb. 2002.

[10] M. Houwing, R. R. Negenborn, M. D. Ilić, and B. D. Schutter, "Model predictive control of fuel cell micro cogeneration systems," in *Proc. IEEE Conf. Netw. Sens. Control*, Okayama, Japan, 2009, pp. 708–713.

[11] L. Jin, R. Kumar, and N. Elia, "Model predictive control-based real-time power system protection schemes," *IEEE Trans. Power Syst.*, vol. 25, no. 2, pp. 988–998, May 2010.

[12] M. Arnold and G. Andersson, "Model predictive control of energy storage including uncertain forecasts," in *Proc. 17th Power Syst. Comput. Conf.*, Stockholm, Sweden, 2011, pp. 954–960.

[13] F. Oldewurtel *et al.*, "Use of model predictive control and weather forecasts for energy efficient building climate control," *Energy Build.*, vol. 45, pp. 15–27, Feb. 2012.

[14] T. Yamaguchi *et al.*, "Model predictive control of car storage battery in HEMS considered car traveling," in *Proc. SICE Annu. Conf.*, Nagoya, Japan, 2013, pp. 1352–1358.

[15] M. U. Kajgaard, J. Mogensen, A. Wittendorff, A. T. Veress, and B. Biegel, "Model predictive control of domestic heat pump," in *Proc. Amer. Control Conf.*, Washington, DC, USA, 2013, pp. 2013–2018.

[16] C. Ziogou, S. Papadopoulou, M. C. Georgiadis, and S. Voutetakis, "On-line nonlinear model predictive control of a PEM fuel cell system," *J. Process Control*, vol. 23, no. 4, pp. 483–492, 2013.

[17] L. M. Monteiro and J. M. Igreja, "On performance of distributed model predictive control in power system frequency regulation," in *Proc. 11th Port. Conf. Autom. Control*, Porto, Portugal, 2014, pp. 71–80.

[18] A. Parisio, E. Rikos, G. Tzamalis, and L. Glielmo, "Use of model predictive control for experimental microgrid optimization," *Appl. Energy*, vol. 115, pp. 37–46, Feb. 2014.

[19] W. Su, J. Wang, K. Zhang, and A. Q. Huang, "Model predictive control-based power dispatch for distribution system considering plug-in electric vehicle uncertainty," *Elect. Power Syst. Res.*, vol. 106, pp. 29–35, Jan. 2014.

[20] V. Spudić, C. Conte, M. Baotić, and M. Morari, "Cooperative distributed model predictive control for wind farms," *Opt. Control Appl. Methods*, vol. 36, no. 3, pp. 333–352, 2015.

[21] T. Suzuki, Y. Goto, T. Terazono, S. Wakao, and T. Oozeki, "Forecasting of solar irradiance with just-in-time modeling," *Elect. Eng. Japan*, vol. 182, no. 4, pp. 19–28, 2013.

[22] H. Homma *et al.*, "PV output prediction under various conditions of time and spatial resolutions by just-in-time modeling," in *Proc. 29th Eur. PV Solar Energy Conf. Exhibit.*, Amsterdam, The Netherlands, 2014, pp. 2904–2907.

[23] Y. Fujimoto, T. Sugiura, and N. Murata, "*K*-nearest neighbor approach for forecasting energy demands based on metric learning," in *Proc. Int. Work Conf. Time Series*, Granada, Spain, 2014, pp. 1–11.

[24] H. Akaike, "A new look at the statistical model identification," *IEEE Trans. Autom. Control*, vol. 19, no. 6, pp. 716–723, Dec. 1974.

[25] M. M. Deza and E. Deza, *Encyclopedia of Distances*, 2nd ed. Heidelberg, Germany: Springer, 2012.

[26] E. P. Xing, A. Y. Ng, M. I. Jordan, and S. J. Russell, "Distance metric learning with application to clustering with side-information," in *Proc. Adv. Neural Inf. Process. Syst.*, vol. 15. Vancouver, BC, Canada, 2002, pp. 505–512.

[27] M. C. Campi, S. Garatti, and M. Prandini, "The scenario approach for systems and control design," in *Proc. 17th World Congr. Int. Fed. Autom. Control*, Seoul, South Korea, 2008, pp. 381–389.

[28] R. Ogata *et al.*, "Economic evaluation of residential energy systems based on prediction—operation planning—control method under time-of-use prices," in *Proc. 28th Int. Conf. Efficiency Cost Optim. Simulat. Environ. Impact Energy Syst.*, Pau, France, 2015, pp. 1–12.

[29] A. Yoshida, K. Ito, and Y. Amano, "Energy-saving evaluation of SOFC cogeneration systems with solar cell and battery," *J. Fuel Cell Sci. Technol.*, vol. 11, no. 6, Dec. 2014, Art. no. 061006.

[30] P. O. Fanger, *Thermal Comfort: Analysis and Applications in Environmental Engineering*. Copenhagen, Denmark: Danish Tech. Press, 1970.

[31] C. Gao and M. A. Redfern, "Automatic compensation voltage control strategy for on-load tap changer transformers with distributed generations," in *Proc. Int. Conf. Adv. Power Syst. Autom. Protect.*, Beijing, China, 2011, pp. 737–741.

[32] S. Kawano, S. Yoshizawa, Y. Fujimoto, and Y. Hayashi, "The basic study for development of a method for determining the LDC parameters of LRT and SVR using PV output forecasting," in *Proc. IEEE PES Conf. Innov. Smart Grid Technol.*, Washington, DC, USA, 2015, pp. 1–5.

[33] Y. Hayashi. (2015). *Development of Distributed Cooperative EMS Methodologies for Multiple Scenario by Using Versatile Demonstration Platform Japan Science and Technology Agency, CREST Program*. [Online]. Available: http://www.jst.go.jp/kisoken/crest/en/project/36/36_05.html

[34] T. Ueno and H. Kitahara, "Development of heat source characteristic model of home use air conditioner—Part 2: Characteristic model for heating period," Central Res. Inst. Elect. Power Ind., Tokyo, Japan, Tech. Rep. R10009, 2012.

[35] *User's Manual for CPLEX*, IBM, Armonk, NY, USA, 2009.

[36] *MATLAB*, Mathworks Inc., Natick, MA, USA, 2015.

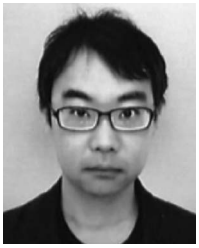

Yu Fujimoto received the Ph.D. degree in engineering from Waseda University, Tokyo, Japan, in 2007, where he is an Associate Professor with the Advanced Collaborative Research Organization for Smart Society. His primary areas of interest are machine learning and statistical data analysis. His current research interests include data mining in energy domains especially for controlling power in smart grids, and statistical prediction of the power fluctuation under the large introduction of renewable energy sources. He is a member of the Information Processing Society of Japan.

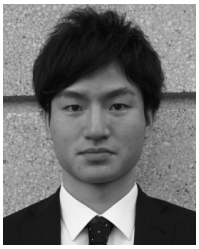

Hiroshi Kikusato received the B.E. and M.E. degrees from Waseda University, Japan, in 2013 and 2015, respectively, where he is currently pursuing the Ph.D. degree. His research interests are optimization of distribution system and voltage control.

Shinya Yoshizawa received the B.E., M.E., and Ph.D. degrees in engineering from Waseda University, Tokyo, Japan, in 2011, 2013, and 2015, respectively, where he is a Research Associate with the Department of Electrical Engineering and Bioscience. His current research interests include operation and control of active distribution systems and smart grids. He is a member of the Institute of Electrical Engineers of Japan.

Shunsuke Kawano received the M.Eng. degree in electrical engineering and bioscience from Waseda University, Japan, in 2014, where he is currently pursuing the Ph.D. degree with the Department of Advanced Science and Engineering. His research interests include voltage control, distribution system, analysis, and distribution system planning.

Akira Yoshida received the B.S., M.S., and D.Eng. degrees in mechanical engineering from Waseda University, Japan, in 2010, 2012, and 2015, respectively, where he is an Assistant Professor with the Department of Applied Mechanics and Aerospace Engineering. He was a Visiting Researcher with the Chair of Application and Middleware Systems, Technical University of Munich, in 2016. His research interests include energy system, energy management, and operations research.

Shinji Wakao was born in Fukuoka, Japan, in 1965. He received the B.E., M.E., and Ph.D. degrees from Waseda University, Tokyo, Japan, in 1989, 1991, and 1993, respectively, where he joined the Department of Electrical, Electronics, and Computer Engineering, in 1996, and became an Associate Professor in 1998. Since 2006, he has been a Professor with the Department of Electrical Engineering and Bioscience, Waseda University. His research interests include electromagnetic field computation, photovoltaic power generation system, and design optimization of electric machines. He is a member of the Institute of Electrical Engineers of Japan and the Japan Solar Energy Society.

Noboru Murata received the B.Eng., M.Eng., and Dr.Eng. degrees in mathematical engineering and information physics from the University of Tokyo, in 1987, 1989, and 1992, respectively. He was with GMD FIRST, Germany, and RIKEN, Japan. Since 2000, he joined Waseda University, Japan, where he is currently a Professor. His research interest includes the theoretical aspects of learning machines such as neural networks, focusing on the dynamics, and statistical properties of learning.

Yoshiharu Amano received the Doctor of Engineering degree in control engineering from Waseda University, in 1998, where he is a Professor with the Faculty of Science and Engineering. He was a Visiting Professor with the Industrial Energy Systems Laboratory, EPFL, Lausanne, Switzerland, in 2008. His research interest includes optimization of energy management systems and systems integration of autonomous robot, and diagnostics of devices utilizing fieldbus technology. He is a member of SICE, ASME, and JSME.

Shin-ichi Tanabe received the degree from the Department of Architecture, Waseda University, in 1982, where he has been a Professor with the Department of Architecture, since 2001. He was with the Laboratory of Heating and Air Conditioning, Technical University of Denmark, from 1984 to 1986, and the Center for Environmental Design Research, University of California at Berkeley, from 1992 to 1993. He was a Guest Professor with the International Centre for Indoor Environment and Energy, Technical University of Denmark, from 2002 to 2003. He is an expert in the fields of indoor air quality, thermal comfort, and energy.

Yasuhiro Hayashi received the B.Eng., M.Eng., and D.Eng. degrees from Waseda University, Japan, in 1989, 1991, and 1994, respectively. In 1994, he became a Research Associate with Ibaraki University, Mito, Japan. In 2000, he became an Associate Professor with the Department of Electrical and Electronics Engineering, Fukui University, Fukui, Japan. He has been with Waseda University, as a Professor of the Department of Electrical Engineering and Bioscience, since 2009, and the Director of the Research Institute of Advanced Network Technology, since 2010. Since 2014, he has been the Dean of the Advanced Collaborative Research Organization for Smart Society, Waseda University. His current research interests include optimization of distribution system operation and forecasting, operation, planning, and control concerned with renewable energy sources and demand response. He is a member of the Institute of Electrical Engineers of Japan and the International Council on Large Electric Systems.